Journal of Drug Delivery Science and Technology 86 (2023) 104752

Contents lists available at ScienceDirect

Journal of Drug Delivery Science and Technology

journal homepage: www.elsevier.com/locate/jddst

Insights into transport in mucus barrier: Exploring particle penetration through the intestinal mucus layer

Mohammad Valibeknejad [a,1], Seyed Majid Abdoli [a], Reza Alizadeh [a], Silvia M. Mihăilă [b], Amir Raoof [c,*]

[a] Department of Chemical Engineering, Sahand University of Technology, Sahand New Town, Tabriz, Iran
[b] Division of Pharmacology, Utrecht Institute for Pharmaceutical Sciences, Utrecht University, Utrecht, the Netherlands
[c] Department of Earth Sciences, Utrecht University, Utrecht, the Netherlands

ARTICLE INFO

Keywords:
Intestinal mucus barrier
Flow hydrodynamic inside the mucus layer
Computational fluid dynamics
Penetration into the mucus layer

ABSTRACT

Nearly all pharmaceuticals and nutrients must cross numerous barriers to gain access and be eliminated from the body. The gastrointestinal mucosa, comprised of specialized epithelial cells layered with mucus, is among the most critical of these barriers. With its intricate structure, this mucus layer facilitates nutrient transport and impedes the transit of toxins and bacteria. The permeability of this mucus layer is key in determining the temporal availability and concentration of various compounds. Numerous methods for enhancing the permeability of select particles through this layer have been examined, employing diverse techniques to quantify the impact of these alterations. However, studies exploring mucus permeability have largely overlooked the potential effect of fluid flow on the mucus layer. In this research, we apply numerical methods to investigate the penetration of particles and drugs through the mucus layer towards the intestinal epithelium, comparing the benefits and distinctions of these methods.

To simulate hydrodynamic effects within the mucus layer, we model intestinal mucus as a Herschel Bulkley fluid, solving the Navier-Stokes equations to simulate fluid flow. These equations are integrated with mass transfer equations to emulate particle penetration through the mucus layer. Our work utilized two different scenarios to simulate the penetration of Brilliant Blue FCF (BFC) into the mucus layer. In the first scenario, molecular diffusion is the sole mechanism responsible for mass transfer. In the second scenario, we also consider convection as an auxiliary mechanism for BFC penetration.

By comparing our simulation outcomes with experimental observations, we demonstrate the necessity of incorporating the convection term to accurately mirror experimental findings. Moreover, we analyzed the effect of varying the diffusion coefficient and viscosity on penetration. The findings revealed that both parameters significantly influence BFC penetration. We also assessed the concentration of drug samples and particles of varying sizes and surface coatings at the epithelial layer. The simulation-based methodology developed in this study shows that internal fluid flow within the mucus layer can profoundly impact particle transport, necessitating the consideration of the convection mechanism for mass transfer in both numerical simulations and penetration analyses.

1. Introduction

1.1. Mucus

Mucus, a viscoelastic aqueous secretion, overlays the epithelial surfaces of the respiratory, vaginal, and gastrointestinal systems, serving as a natural lubricant and a selective barrier against pathogens and particles [1–5]. The key functional constituent of mucus is mucin, a highly glycosylated protein of substantial molecular weight (10–40 MDa) [6]. Mucin, a negatively charged protein, boasts oligosaccharide side chains inclusive of terminal sialic acid and sulfate residues [7]. Mucin proteins, interconnected covalently (via disulfide bonds) and non-covalently

* Corresponding author.
E-mail addresses: m.valibeknejad@gmail.com, m.valibeknejad@uu.nl (M. Valibeknejad), abdoli@sut.ac.ir (S.M. Abdoli), r.alizadeh@sut.ac.ir (R. Alizadeh), s.mihaila@uu.nl (S.M. Mihăilă), a.raoof@uu.nl (A. Raoof).
[1] Present address: Utrecht University, Utrecht, the Netherlands.

https://doi.org/10.1016/j.jddst.2023.104752
Received 17 January 2023; Received in revised form 22 June 2023; Accepted 9 July 2023
Available online 10 July 2023

(through hydrophobic and electrostatic interactions, hydrogen bonds, and physical entanglements), form large polymeric sheets creating the mesh-like structure of the mucus [1,8]. Interstitial spaces between the mucin fibers (0.2–5.0 wt %) accommodate water (95 wt %), proteins (0.5 wt %), salt (0.5–1.0 wt %), lipid (1–2 wt %), DNA, and cells [2]. Mucus is secreted by goblet cells [9] and is subsequently digested, recycled, or discarded [10].

1.2. The intestinal mucus layer

The intestinal mucus layer, a protective coating of epithelial cells, forms the gastrointestinal (GI) barrier. This system allows the absorption of nutrients, pharmaceuticals, and other compounds into the circulatory system. It provides a safeguard against infection [10], and it traps toxins and bacteria to prevent their penetration into the epithelium [11]. This mucus layer covers both the small and large intestines. In the small intestine, the mucus layer is a monolayer. However, in the large intestine, it is divided into two layers. The outer layer, being less dense, permits bacteria passage, while the inner layer, which is firmly attached to the epithelium, is denser and relatively impenetrable. The inner mucus layer's mesh-like structure and small pore sizes deter bacterial penetration [8,12]. This mucus layer is constantly removed and regenerated, typically every 50–270 min [4,13], to maintain a protective barrier whose characteristics, such as viscosity, pH, and composition, vary based on anatomical position. The thickness of this mucus layer differs considerably among and within bodily organs, with the thicknesses within the gastrointestinal system displayed in Table 1.

1.3. The intestinal mucus as a barrier

Jointly, the epithelial and mucus layers constitute the intestinal barrier. These layers exercise selective control over the transport of molecules, particulates, and microorganisms to the underlying epithelial layer, employing mechanisms such as size restriction, covalent bonding, hydrophobic and electrostatic affinities, and other specific interactions [4,8,10]. Given these filtration mechanisms, the degradation of the mucus barrier poses a significant challenge in the fields of medicine and food development. Before proceeding to in vivo experiments, the ability of substances to cross this barrier should be assessed using preclinical in vitro and in silico models [10,18].

1.3.1. In-vitro study of the mucus barrier

The structure, composition, and dynamic behavior of mucus are suitably mimicked in animal models, albeit with the challenge of nanoparticle tracking [5]. The chamber system, simulating a static condition, is a widely accepted model for scrutinizing drug transport across the intestinal barrier (as shown in Fig. S. 1. A in the Supplementary Material) [19]. This static model adequately provides preliminary data regarding the potential of chemicals and particles to breach the mucus barrier. In this setup, a chamber divided by membranes accommodates mucus injected between these membranes. A nanoparticle solution is introduced on the apical side, allowing particles to diffuse across the mucus and be gathered on the basolateral side. The concentration of drugs in both the apical and basolateral sections can be determined through various analyses, such as radioactive detection, fluorescent spectrometry, or high-performance liquid chromatography [19]. This model, however, often lacks the physiological stimuli induced by shear stress. As a result, some compounds with limited residence time on the lumen side cannot penetrate the mucus layer [20].

Recently, microfluidic tools with mucus integration have been developed to overcome the limitations of the static system (refer to Fig. S. 1. b in the Supplementary Material) [5,18,21–23]. In a fluidic setup akin to the chamber model, the nanoparticle solution flows on the apical channel, and diffusing particles are captured in the basolateral compartment [18]. Several methods, including MPT, FRAP, bulk diffusion, and penetration studies, can illustrate particle penetration over time [19,24] (for more information on visualization and measurement of penetration across the mucus layer, please refer to Supplementary Material Section 2). Various image analysis algorithms can then quantify particle penetration and the diffusion coefficient [25].

The use of microfluidic setups requires small amounts of mucus and nanoparticles (representing drugs and nutrients). This approach guarantees a consistent configuration by controlling the flow structure and flow rate to simulate the in vivo mucus environment. Furthermore, it provides a precise method for assessing compound permeability across a mucus layer, offering automation options and suitability for a broad spectrum of applications [5,18].

Elberskirch et al. designed microfluidic systems to study the intestinal mucus barrier with a fluidic basolateral side [18]. However, these studies inadequately considered the impact of the flowing lumen material and shear stress. Jia et al. crafted a microfluidic system to examine the penetration of nanoparticles into a purified mucus solution (refer to Fig. 1). In this system, the mucus and nanoparticle solution were separated using pillars positioned between channels [5]. This device was later refined by Wright, Wignall et al. to explore the penetration of variously modified particles in the mucus layer [26].

1.3.2. Employing CFD-based techniques to estimate the mucus barrier

Computational Fluid Dynamics (CFD) modeling can help reduce the reliance on expensive and technically demanding experimental research. CFD aids in developing efficient experimental setups by modeling the parameters involved in fluid dynamics, such as those in intestinal barrier studies. The delivery of nutrients to the surfaces of the gut villi is crucial for nutrient absorption in the intestinal tract. In the intestine, mixing, which homogenizes heterogeneous systems, occurs on

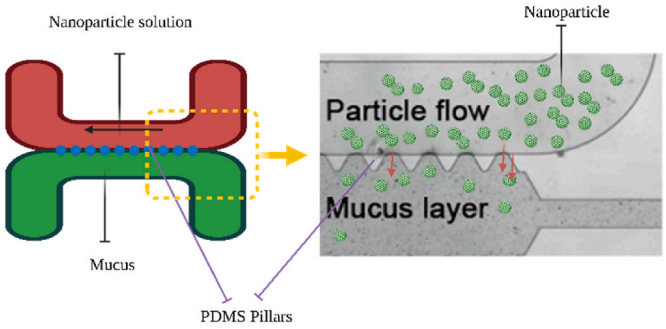

Fig. 1. A schematic representation of the mucus-on-chip device used by Jia et al. (Reproduced whit BioRender by permission from Ref. [5]) to investigate particle penetration through the mucus layer using purified mucin (porcine intestine mucin, type III). A dye or nanoparticle solution is pumped into the lumen channel at a constant flow rate, and particle penetration through the mucus layer is visualized. The capacity of BFC (Brilliant Blue FCF) to cross the mucus barrier was studied using this device [5].

Table 1
Mucus layer thicknesses in the rat gastrointestinal tract [14], human intestine [15,16], and mucins type for the human GI tract [17].

	Duodenum (rat)	Jejunum (rat)	Ileum (rat)	Colon (rat)	Small intestine (human)	Colon (human)
The thickness of the mucus layer (μm)	170	123	480	830	15.5	600
Mucin types in human	MUC2 MUC6	MUC2	MUC2	MUC2 MUC5B		

various scales: macromixing transpires at scales comparable to the intestinal diameter, whereas diffusional mixing takes place on a smaller microscale. Most CFD analyses have concentrated on identifying intestinal wall movements that facilitate adequate mixing, nutrient absorption, and chyme flow in the gut [27–33]. To the best of the author's knowledge, this work represents the first numerical study of intestinal mucus. However, numerous numerical studies have been conducted on respiratory tract mucus. Alex et al. employed CFD to investigate pharmaceutical adsorption and mucus clearance in the nose, probing particle penetration in the mucus layer using the advection-diffusion equation [34]. Molecular dynamic simulations have been utilized to examine particle diffusion in the mucus layer and the effect of particle size and surface coating [35]. Machine learning has been used to predict the permeability and fate of particles in airway mucus [36], and mucociliary clearance has been studied, considering airway mucus as a power law, thixotropic [37], and Herschel Bulkley fluid [38].

1.4. Objective of this study

Designing medications and drug carriers capable of successfully crossing the mucosa necessitates an in-depth understanding of the biological hurdles involved [10]. The mucus layer constitutes the final barrier between digested food or orally administered pharmaceuticals and the epithelium [39]. Various in vitro, in vivo, and ex vivo methods have been employed to elucidate the role of mucus as a barrier to particle penetration [19]. However, the data obtained from these models are often limited due to their unpredictability and the challenges involved in adapting them to basic transport phenomena. Numerical modeling can complement these studies by illuminating the underlying processes. This study presents a numerical method for investigating mucus barriers based on transport phenomena, wherein fluid flow and mass transfer equations are combined to simulate particle transport into the mucus layer. Ultimately, we compare the simulation results with experimental observations from the literature to determine an appropriate mass transport mechanism (between diffusive and diffusive convective mechanisms).

2. The modelling approach

The primary objective of this study is to simulate the barrier function of the mucus layer using computational models. To do this, fluid flow and mass transfer equations need to be solved to simulate BFC penetration across the mucus layer. In the model, mucus is treated as a Herschel Bulkley fluid, and the lumen material is treated as a Newtonian fluid. The following section details the numerical approach.

2.1. Governing equation

2.1.1. Fluid flow equation

For determining the velocity and pressure fields of the viscose fluid, continuity (1) and Navier-Stokes (2) are solved together [40].

$$\frac{\partial \rho}{\partial t} + \nabla.(\rho \boldsymbol{U}) = 0 \tag{1}$$

$$\rho(\boldsymbol{U}.\nabla)\boldsymbol{U} = \nabla.\left[-\boldsymbol{P} + 2\mu\left(\nabla \boldsymbol{U} + (\nabla \boldsymbol{U})^{T}\right)\right] \tag{2}$$

Where ρ is the fluid density, μ is the viscosity, P is the pressure, and U is the velocity field.

The lumen material is treated as a Newtonian fluid; in this case, μ represents the water viscosity. Maria et al. demonstrated that the Herschel Bulkley model could accurately fit the rheological analysis of mucus [41]. Galko et al. simulated the fluid flow in the mucus layer in the respiratory tract as a Herschel Bulkley fluid [38]. Here, we also treat mucus as a Herschel Bulkley fluid, where μ is calculated using equation (3) [40].

$$\mu = \frac{\tau_y}{\dot{\gamma}}\left(1 - \boldsymbol{exp}\left(-\boldsymbol{m}_p\dot{\gamma}\right)\right) + \boldsymbol{m}\left(\frac{\dot{\gamma}}{\dot{\gamma}_{ref}}\right)^{n-1} \tag{3}$$

where τ_y is the yield stress, $\dot{\gamma}$ is the shear rate, m_p is the model parameter, m is the Apparent viscosity, $\dot{\gamma}_{ref}$ is the reference shear rate, and n is the Flow index coefficient. These equations ((1), (2), and (3)) can be used for laminar flow. This is a valid assumption as the Reynolds number in the GI tract is less than 200 [28].

2.1.2. Mass transfer equation

The mass conservation equation was used to determine the concentration of particles in both the mucus and lumen sides. For the transport of particles, diffusion (the second term on the left-hand side of (4)) and convection (the third term on the left-hand side of (4)) mechanisms are considered. The concentration of particles in a homogenous fluid is calculated by (4) as:

$$\frac{\partial \boldsymbol{C}_i}{\partial t} + \nabla.(-\boldsymbol{D}_i\nabla \boldsymbol{C}_i) + \boldsymbol{U}.\nabla \boldsymbol{C}_i = \boldsymbol{R}_i \tag{4}$$

where C_i is the concentration of component i, D_i is the diffusion coefficient for homogenous fluid, R_i is the reaction term, and U is the velocity field.

2.2. Model geometry

Fig. 1 shows the setup used by Jia et al. [5]. The mucus-on-chip device consists of two channels, each 10 mm long, 1250 μm wide, and 130 μm high. Pillars positioned in the center of the microfluidic setup separate the lumen and mucus channel materials [5]. In this study, we use the same geometry to compare the simulation results with experimental observations (Fig. 2). Given that both channels in the mucus-on-chip device are situated side by side, PDMS (Polydimethylsiloxane) pillars are used to segregate the mucus from the lumen-side material. In these systems, where surface forces are more dominant, phase guide pillars produce sufficient capillary forces to retain the mucus in the correct channel. A model with similar geometry is utilized, referred to as the partial contact model (shown in Fig. 2b). In the design shown in Fig. 2a, a complete interface between mucus and lumen material is created for particle penetration (referred to as the full contact model). The full contact design is used to simulate conditions as close to in-vivo as possible. The thickness of the mucus layer in both the mucus-on-chip device and this study is set at 1250 μm.

2.3. Simulation parameter and boundary condition

Table 2 provides the parameter values used for numerical modeling. The method of selecting these parameters is explained in the following sections.

2.3.1. Diffusion coefficient

BFC is a low molecular weight (MW = 792.85) molecule that can freely diffuse into the mucus [5]. The diffusion coefficient in water can approximate the diffusion coefficient of this molecule in the mucus layer [44].

2.3.2. Mucus density

To the best of the writer's information, the density of GI mucus is not explored in the literature. In this study, as an approximation, we used the density of respiratory tract mucus provided by Lafforgue et al. (5) [45].

$$\rho = -1.4145\varphi^2 + 7.45\varphi + 1006.6 \tag{5}$$

where φ is the mucin weight percentage.

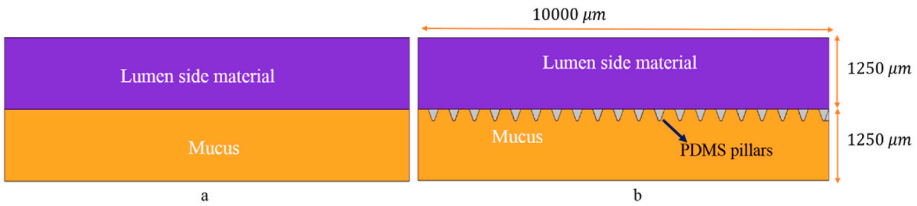

Fig. 2. The microfluidic geometry used to simulate the experimental observations of mucus on chip study of Jia et al. a) the full contact model, and b) the partial contact model where the separation between the lumen and mucus domains are created using solid PDMS pillars.

Table 2
The physical properties used in numerical modeling.

Lumen	Density [kg/m^3]	1000		[42]
	Viscosity [Pa.s]	1×10^{-3}		[43]
	Diffusion coefficient [m^2/s]	56.8×10^{-11}	Brilliant blue FCF	[44]
Mucus	Density [kg/m^3]	1006	ρ	[45]
	yield stress [Pa]	0.0146	τ_y	[41]
	Model parameter [sec]	10	m_p	[41]
	Apparent viscosity [Pa.s]	0.0102	m	[41]
	Reference shear rate [1/sec]	1	$\dot{\gamma}_{ref}$	[41]
	Flow index coefficient [−]	0.9651	n	[41]
	Diffusion coefficient [m^2/s]	56.8×10^{-11}	Brilliant blue FCF	[44]

2.3.3. Mucus viscosity

The rheology of mucus impacts the passage of nutrients, medications, and pathogenic agents across the mucus layer and affects its hydration and lubricating characteristics. At the macroscopic level, mucus behaves like a non-Newtonian viscoelastic fluid, displaying viscous (flowing) and elasticity (resistance to deformation) properties. At the microscale (i.e., pore scale), mucus behaves as a low-viscosity fluid. Under small shears, mucus has a viscosity of about 100–10,000 times that of water. When shear rates approach maximal physiological rates, mucus acts like a shear-thinning fluid with viscosity values similar to water. The rheology of mucus has been studied in native and purified mucin in several animals [9,10]. For a recent review, see Refs. [1,46,47]. Purified mucin (i.e., porcine intestine mucin, type III) was used as a mucus model in the mucus-on-chip device [5]. Maria et al. investigated the rheological characteristics of pig gastric mucin solutions [41]. In our study, we use the characterization parameters of the Herschel Bulkley models fitted to the study by Maria et al.

2.3.4. Boundary condition

Boundary conditions are crucial in numerical modeling to represent interactions with surrounding boundaries. Simulations are conducted at atmospheric pressure and body temperature (i.e., 37 °C). Mucus is positioned in the channel with a closed end. The lumen material is injected into the lumen channel at a constant velocity and discharged at the outlet under atmospheric pressure. The flow of lumen material exerts a shear force on the mucus, causing movement. Continuity conditions are applied at the interface between the mucus and lumen channels; stress, velocity, and mass flux are continuous from one fluid to another (represented by equations (6)–(8) for stress, velocity, and mass flux, respectively).

$$(\tau_{lumen\_side} = \tau_{mucus\_side})_{|interface} \tag{6}$$

$$(\boldsymbol{U}_{lumen\_side} = \boldsymbol{U}_{mucus\_side})_{|interface} \tag{7}$$

$$(\boldsymbol{J}_{lumen\_side} = \boldsymbol{J}_{mucus\_side})_{|interface} \tag{8}$$

Here, τ is the stress tensor, U is the velocity component, and J is the mass transfer flux. Nanoparticles enter the lumen channel at a constant concentration and permeate through the mucus due to the concentration gradient and induced flow field. The boundary conditions used in the simulation are shown in Fig. 3. In this study, COMSOL Multiphysics was utilized to solve the coupled equations.

3. Results

Simulations are carried out for two scenarios, one with partial and one with full contact between mucus and lumen sections. Furthermore, two types of simulations are executed for each scenario. One with diffusive and one with mixed (i.e., diffusive and convective) transport to examine the effect of convective mass transfer. In the mixed transport case, the convection mechanism is facilitated by the induced shear stress from the lumen material. A mass movement from a high-concentration area to a low-concentration area is known as a diffusion (diffusive) mass transfer mechanism. Mass transfer in response to the bulk flow motion is a convective mechanism. Both mucus and lumen material (solution of water and BFC) are treated as incompressible fluids. Fluid flow equations are solved in stationary mode, and mass transfer equations in time-dependent mode. Numerical mesh quality was verified based on the COMSOL average and minimum mesh quality (Table 3). Mesh independency was confirmed by increasing mesh density by ~35% and invariant results (<1%). Further details about mesh independency and mesh quality are provided in the Supplementary Material (Section 3).

3.1. Velocity distribution

The Navier-Stokes equations are solved alongside the continuity equations to obtain the velocity distributions. The results of simulations for velocity fields are shown in Fig. 4. Mass transfer equations are solved in two different scenarios. In the first case, mass transfer only by diffusion is considered within the mucus channel, and in the second case, mass transfer with both diffusion and convection is considered in the mucus channel. Both convection and diffusion processes are considered for the lumen channel in all cases. The velocity distribution, used to calculate convective mass transfer, is computed using fluid flow equations. The results of the simulation for mass transfer equations with streamlines of mass flow (white arrows) for full and partial contact modes are shown in Fig. 5 and Fig. 7, respectively.

As depicted in Fig. 4, the velocity magnitude in the lumen channel is larger than that in the mucus channel (shown as colored surface plots) due to lower viscosity in the lumen fluid. The maximum velocity occurs at the center of the channel, away from the channel walls, where a no-slip boundary condition is applied, and velocity near the wall approaches zero. Shear stress from the flowing lumen material induces flow within the mucus layer at the lumen-mucus interface. The viscosity of the mucus material is larger than the lumen, and thus mucus shows more resistance to flow. PDMS pillars (commonly used in microfluid studies) create additional resistance to flow in the partial contact mode and less direct friction between the lumen and mucus layers. Consequently, velocity magnitudes for partial contact scenarios are smaller under the same flow conditions compared to the full contact simulation mode. Moreover, the presence of pillars affects the tortuosity of the induced flow lines within the mucus layer (as shown using white

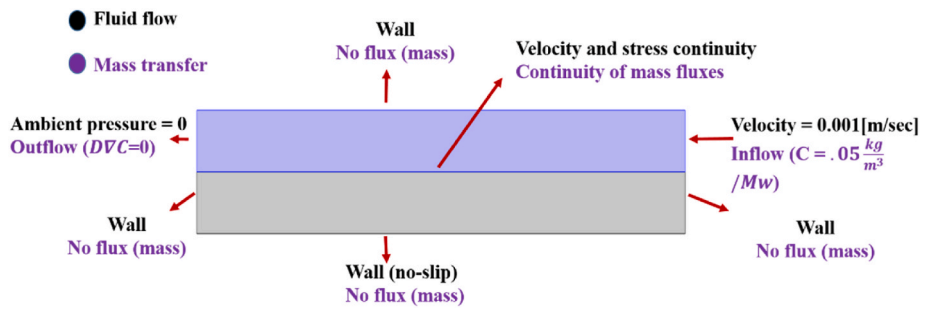

Fig. 3. The set of boundary conditions used for numerical simulations. For all boundaries, black colors show boundary conditions for fluid flow and purple color for mass transfer. (For interpretation of the references to color in this figure legend, the reader is referred to the Web version of this article.)

Table 3
The numerical mesh statistics of the developed model.

Full contact	Mesh type	Structured
	Number of elements	19800
	Minimum element quality (0–1)	1
	Average element quality (0–1)	1
Partial contact	Mesh type	Unstructured (Triangle)
	Number of elements	44491
	Minimum element quality (0–1)	0.61
	Average element quality (0–1)	0.90

arrows), influencing mass transport and mixing in the mucus layer.

3.2. Evolution of the concentration fields

The concentration field evolves over time. Fig. 5 displays 2D concentration profiles for simulations with diffusive and mixed transport scenarios at different times. When only diffusion is present, particle transport occurs solely due to concentration gradients. For mixed transport scenarios, convection also impacts transport alongside diffusion. Here, convective mass transfer improves transport and penetration depth. The local concentration gradients created by the flow's shear effects bring areas of low and high concentration together, generating more significant concentration gradients and producing larger diffusive fluxes. Fig. 6 presents the concentration along the vertical cross-section inside the mucus channel near the right boundary. From this figure, it's evident that the concentration is higher in cases where convection is taken into account, compared to the diffusion cases.

Fig. 7 displays results for the partial contact mode (i.e., in the presence of pillar barriers). Intriguingly, although the behaviors for simulations involving only diffusion are somewhat similar (between partial and full contact scenarios), the mixed transport mode is far more sensitive to the presence of barriers. In the full contact case, penetration occurs more swiftly due to contact effects and considerable velocity magnitudes. When comparing the results of simulations with the mucus-on-chip device results (Fig. 8), the mixed transport mode provides a more realistic behavior, showing that the induced velocity had a significant contribution to the mucus-on-chip results observations. The numerical model can simulate a more realistic situation without placing pillars between the lumen and the mucus layers to predict concentration penetration depths. As illustrated in Fig. 5, it's expected that experiments would have displayed deeper concentration penetrations when there is full contact between the lumen and mucus sections. The white arrows in Figs. 5 and 7 indicate mass flow streamlines for partial and full contact modes with diffusive and mixed (convective and diffusive) mass transfer mechanisms. In diffusion cases, the mass lines in the mucus layer are nearly vertical, indicating that penetration occurs normally to the lumen mucus interface, and there's no convective flux to alter the mass lines.

3.3. Sensitivity analysis

Mucus is a complex gel, and its properties vary with location (i.e., from point to point in the same organ), the number of enzymes and bacteria, and the domain pH [4]. Therefore, the transport parameters aren't fixed and can vary in different situations. To study the effect of these uncertainties, a sensitivity analysis is performed. The penetration depth within the mucus layer is chosen as a target measure to compare different simulations with different parameters. The penetration depth is

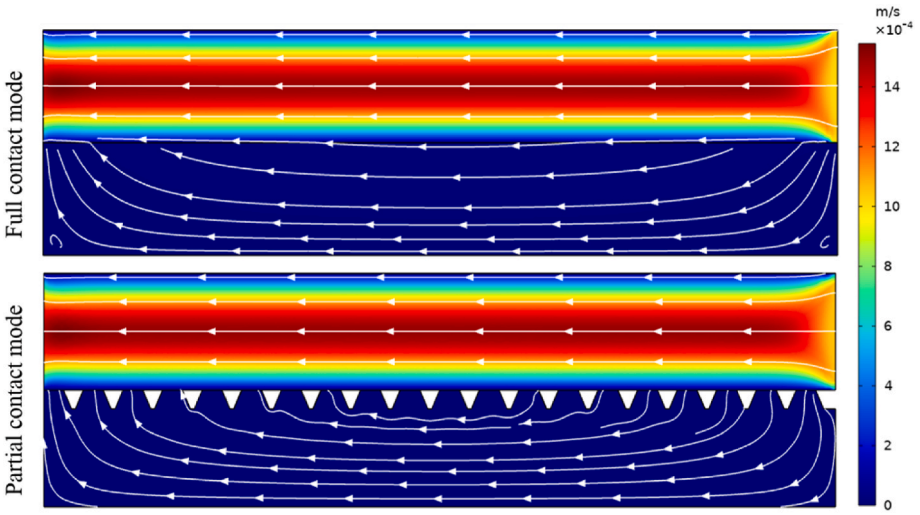

Fig. 4. Velocity distribution (colored surfaces) and velocity streamlines (white lines with arrows) for full and partial contact scenarios.

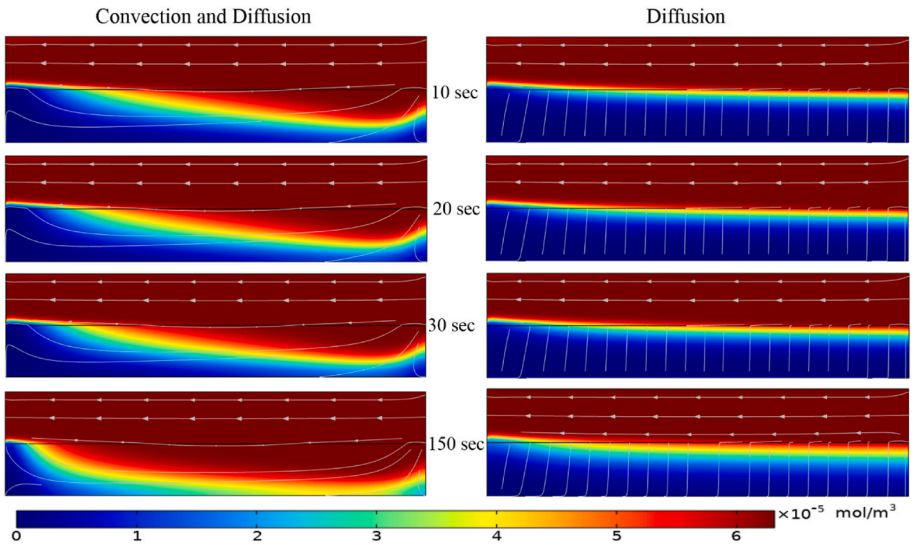

Fig. 5. Concentration profiles (colored surfaces) together with mass lines (white line with arrows) for full contact scenarios.

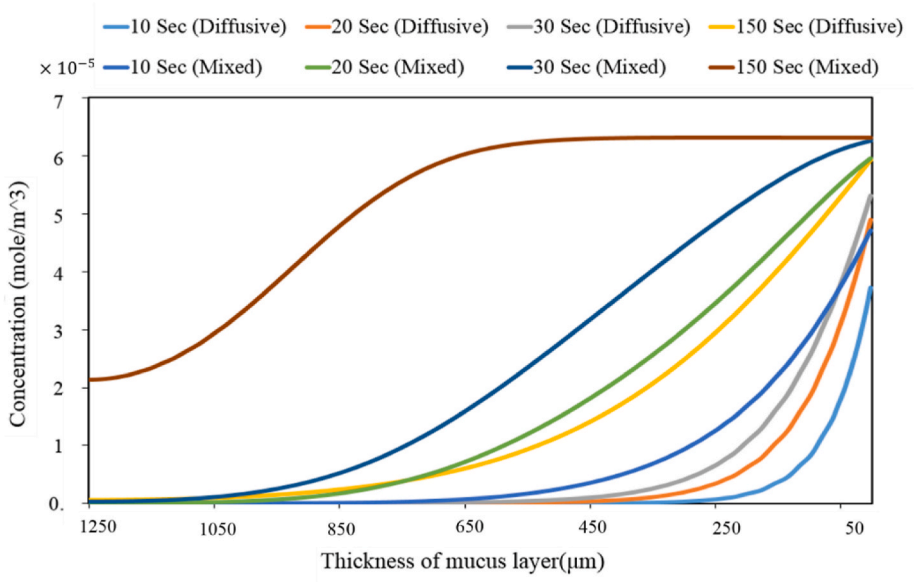

Fig. 6. Concentration along a vertical cross-section (in the mucus channel) for all cases and times shown in Fig. 5.

defined as the largest distance from the contact interface where the concentration of particles is half the concentration of the particles at the lumen inlet (which is also the location of maximum concentration).

Fig. 9 presents the results of the sensitivity analysis. The parameters varied were the diffusion coefficient in mucus and the parameters in the Herschel Bulkley models. The diffusion coefficient was varied by ±25% from its initial value. For the Herschel Bulkley parameters, three sets of parameters were used, which are listed in Table 4. These parameters were selected based on the study of Maria et al., which provides values for different pH levels [41].

The established flow in the lumen channel also prompts the mucus to move, impacting the transport within the mucus layer. The magnitude of the velocity in the mucus layer depends on the mucus viscosity. Fig. 9a illustrates the effect of varying mucus viscosity on the penetration depth of particles (BFC). As viscosity decreases, resistance to flow reduces, and larger velocities are generated in the mucus channel, resulting in more rapid mass transport. Fig. 9b displays the impact of the diffusion coefficient of BFC in the mucus layer on the penetration depth. To study the effect of the diffusion coefficient, only the diffusion mechanism is considered. As anticipated, the penetration depth increases with the diffusion coefficient. A 25% increase in the diffusion coefficient resulted in a 12% increase in penetration in the mucus layer.

3.4. *Coupling of the convective and diffusive fluxes*

The simulations incorporating the convection term have been observed to align best with the microscopic findings. Utilizing numerical simulations, it is possible to determine the contributions of the convection and diffusion fluxes to the total mass flux. Fig. 10 displays the mass transfer fluxes resulting from each convection and diffusion process, obtained by averaging all numerical cells situated in the mucus channel. The results indicate that the induced convection mechanism plays a significant role in transport within the mucus layer. The strength of the convective flux relies on velocity and, therefore, viscosity. Table 5 provides the values of convective and diffusive fluxes for varying diffusion coefficients and Herschel Bulkley parameters.

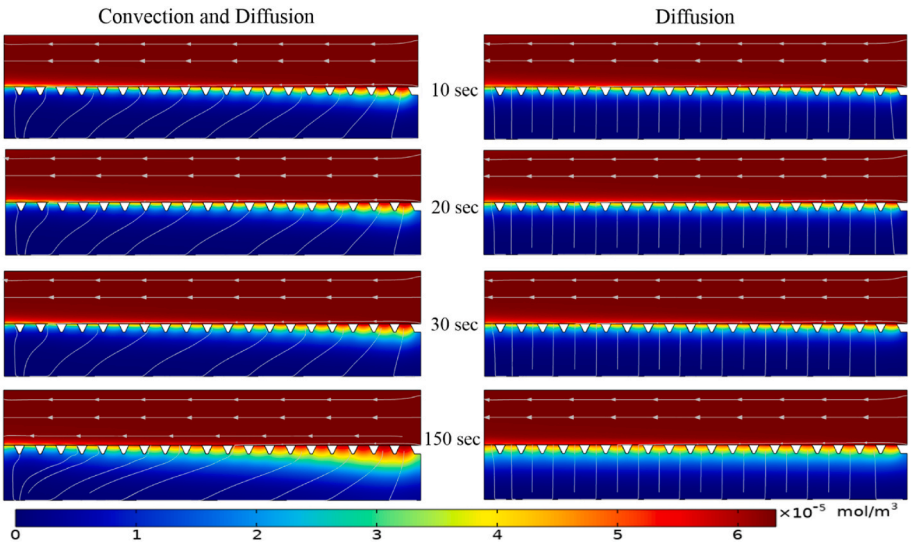

Fig. 7. Concentration profiles (colored surface) and mass lines (white arrows) for partial contact mode where the mass exchange takes place only at the gap locations (i.e., the space between pillars) along the interface.

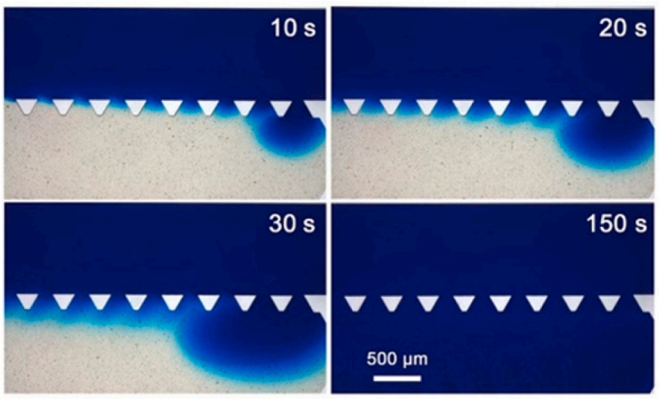

Fig. 8. Penetration of BFC as a low molecular weight particle in the mucus layer from the mucus-on-chip device (adapted by permission from Ref. [5]). The white triangles are barriers (i.e., the PDMS pillars) created during the microfluidic fabrication to provide stable microchannels for fluid flow.

3.5. *Investigation of the drug availability at the epithelial layer surface*

The penetration of three drugs was investigated to assess the drugs' ability to infiltrate the mucus layer (more information regarding the component and numerical methodology is provided in Supplementary Material Section 4). Fig. 11a presents the concentration of the three drugs over time, signifying the drugs' ability to permeate through the mucus layer. Beyond the mucus layer, the drug must traverse the epithelial barrier. Greater drug concentration at the epithelial surface leads to more diffusion through the epithelial layer. Fig. 11a demonstrates that Phenolphthalein has a higher diffusion rate compared to NAC (Nicotinamide adenine dinucleotide), which has a high concentration at the epithelial surface. To observe the impact of particle size on availability at the epithelial layer surface, the penetration of polystyrene nanoparticles of two different sizes was investigated (the methodology is described in Supplementary Material Section 4). Fig. 11b illustrates the effect of nanoparticle sizes on the drug concentration at the epithelial surface over time. From the figure, it is apparent that particles of smaller size exhibit stronger diffusion and a higher concentration. Several methods can augment the permeation of particles into the mucus layer,

Table 4
Characteristic parameters of Herschel Bulkley models for sensitivity analysis.

	Apparent viscosity [Pa.s]	Yield stress [Pa]	Flow index coefficient [−]		
Case1	0.0102	0.0146	0.9651	pH 1.2	[41]
Case2	0.0148	0.0578	0.8978	averaged	
Case3	0.0194	0.1010	0.8306	pH 6.8	[41]

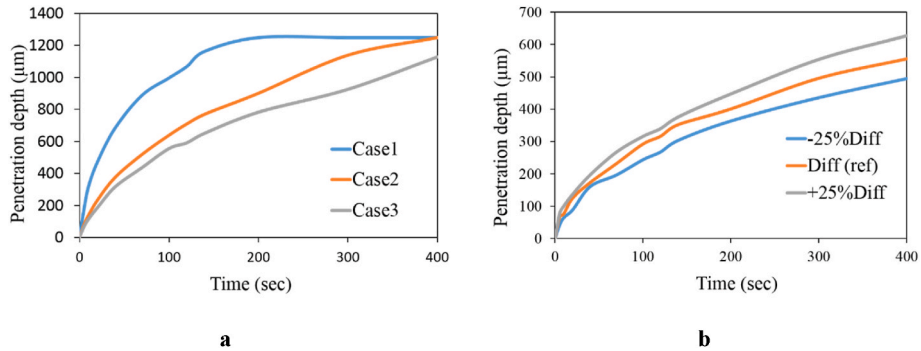

Fig. 9. Effect of Herschel Bulkley parameters (a) and diffusion coefficient (b) on the penetration depth. The values of Herschel Bulkley parameters for the three cases are provided in Table 4. For the diffusion coefficient, ±25% deviation from the initial state (Diff) is considered.

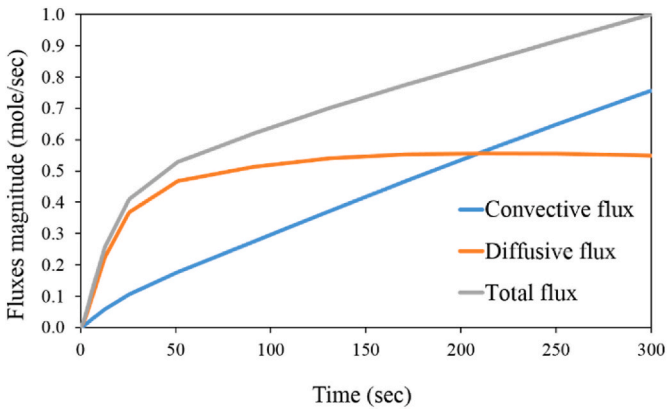

Fig. 10. Average fluxes within the mucus channel (i.e., average over numerical cells within the mucus layer) over time for convective and diffusive mechanisms. Fluxes are presented in normalized form using the maximum flux magnitude of 4.05×10^{-11} [mole/sec]).

Table 5
Values of convective and diffusive fluxes in simulations with partial and full contact scenarios.

			Convective Flux (%)	Diffusive Flux (%)
Partial contact	Effect of Herschel Bulkley parameters	Case1	23.77	76.23
		Case2	6.88	93.12
		Case3	3.97	96.03
	Effect of the diffusion coefficient	−25% Diff	71.81	28.19
		Diff (ref)	76.20	23.77
		+25% Diff	79.07	20.93
Full contact	Effect of Herschel Bulkley parameters	Case1	97.00	3.00
		Case2	84.00	16.00
		Case3	77.00	33.00
	Effect of diffusion coefficient	−25% Diff	97.84	2.16
		Diff (ref)	97.21	2.79
		+25% Diff	96.67	3.33

one of which is PEGylation [48]. A simulation of PEG-modified particles was conducted to observe the effect of PEG-modified particles on their availability (more information regarding this simulation is provided in Supplementary Material Section 4). As demonstrated in Fig. 11b, the concentration of these particles is greater than the polystyrene particle of the same size.

4. Discussion

The investigation of new drugs requires both in-vitro and in-silico testing before proceeding to in-vivo trials. In-silico methods are often preferred due to their cost-effectiveness and reproducibility [49]. However, the precision of these numerical approaches heavily relies on the accurate definition of the mathematical model's physiochemical properties and the exact boundary conditions. Initially, we utilized the same geometry as the in-vitro study conducted by Jia et al. demonstrating that our selected modeling approach can approximate the results observed experimentally. Using PDMS pillars between the two channels is one restriction inherent in in-vitro studies. After validating our modeling approach, we adopted the same model sans pillars to approximate more closely the in-vivo (in-body) situation. As shown by the results from the full-contact case modeling, the use of pillars affects the penetration into the mucus layer.

Another limitation of in-vitro studies involves accurately considering the mucus layer thickness. As mentioned earlier, mucus layer thickness varies throughout the intestine. Achieving a mucus layer thickness of 15 μm (typical of the human small intestine) is challenging. With the approach presented here, it's possible to study mucus barriers of any thickness given the known physiochemical parameters (such as diffusion coefficient, viscosity, and density). This evidence supports the move towards in-silico studies to predict drug availability in the context of physical barriers.

Mucus rheology depends on several factors, including the specific intestinal section, the type of mucin protein, various diseases (human bronchial epithelial mucus and cystic fibrosis mucus [50]), and the number of bacteria [1,46,47]. Sensitivity analyses for viscosity at different pH levels show that viscosity is a crucial parameter in mucus barrier studies. This highlights the need for a comprehensive and accurate rheological model. Having precise viscosity models will assure the accuracy of the in-silico model. Our sensitivity analysis also demonstrated the effect of the diffusion coefficient on transport across the mucus layer. This relationship depends on particle size, surface properties, and the interactions between particles and mucins. Several well-established techniques can measure the diffusion coefficient through the mucus layer [51,52]. These setups can measure the diffusion coefficient for different particles in terms of size, surface modification, and various mucus models. Given the diffusion coefficient and mucus rheology, the approach provided can predict penetration through the mucus layer in the entire intestine.

The in-silico study of drug uptake through the intestine is a multi-scale problem and needs to consider several mechanisms. Initially, an available digestion model should be solved to calculate the drug's availability and concentration in the small intestine [53,54]. Then, the hydrodynamics of flow on the lumen side of the intestine and available

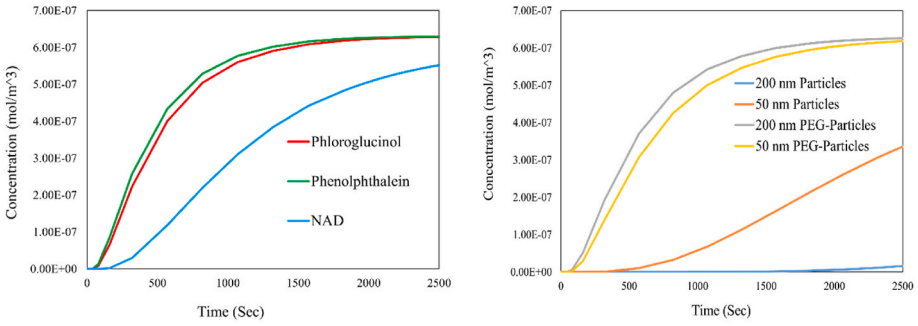

a b

Fig. 11. Sum of concentration along the epithelial surface (lower boundary condition). a) concentration versus time for three different drugs. b) concentration versus time for particles with 50 and 200 nm sizes and PEG-modified particles.

models for mixing considering factors such as contraction, peristalsis, and the effect of villi should be addressed [55–58]. At this stage, we have the particle concentration and flow velocity (shear stress) at the interface of the lumen and mucus. Our research can be applied to model the fluid flow and penetration through the mucus layer. The next step involves considering diffusion through the epithelial layer and absorption into the blood vessels.

5. Conclusions

Numerical simulation complemented the findings from wet lab experimental tests examining mucus barrier function and permeability. In order to simulate the mucus barrier, transport equations (including momentum and mass) were numerically resolved. For fluid flow equations, viscosity is the determinant parameter, thereby majorly controlling the flow regime and velocity magnitude. For mass transfer equations, both diffusion and convective mechanisms were considered. The diffusion coefficient is pivotal for the diffusive mechanism, while fluid velocity is key for the convective mechanism.

In this study, mucus was treated as a Herschel Bulkley fluid, and it was shown that the applied method could accurately predict experimental particle penetration into the mucus layer. Moreover, it was demonstrated that diffusion and convection should be seen as synergistic/complementary driving forces of mucus penetration. Results indicated that the induced flow in the lumen section, situated atop the mucus layer, significantly influences particle transport within the mucus layer. This effect is contingent upon the fluid velocity within the mucus layer. The induced velocity within the mucus layer relies on mucus viscosity.

By employing a sensitivity analysis, we demonstrated that the fraction of particle transport via the convection mechanism diminishes with increased viscosity. Herein, we developed a modeling-based technique to simulate particle penetration into synthetic mucus (porcine intestine mucin, type III). The mucus layer thickness used in this study is greater than that in the human intestine due to the larger mucus layer thickness used in microfluidic experiments. The main objective of this study was to verify the chosen numerical approach and the role of major transport parameters in particle penetration and to identify the mass transfer mechanisms. The method developed can simulate the penetration of particles of different sizes and surface coating into the mucus layer. Moreover, various mucus models and precise thicknesses can be utilized for the mucus layer. In sum, we developed an enhanced computational method to model particle penetration, which holds implications for the mucus layer.

CRediT authorship contribution statement

Mohammad Valibeknejad: Investigation, Methodology, Visualization, Validation, Writing– original draft. **Seyed Majid Abdoli:** Conceptualization, Supervision, Writing - review & editing. **Reza Alizadeh:** Conceptualization, Supervision, Writing - review & editing. **Silvia M. Mihăilă:** Conceptualization, Supervision, Writing - review & editing. **Amir Raoof:** Conceptualization, Supervision, Software, Writing - review & editing.

Declaration of competing interest

The authors declare that they have no known competing financial interests or personal relationships that could have appeared to influence the work reported in this paper.

Data availability

Data will be made available on request.

Acknowledgments

The authors express their deep gratitude to Yvonne Vercoulen, Karin Strijbis, Noortje IJssennagger, and Maitrayee Chatterjee of the University Medical Centre Utrecht, Utrecht University, The Netherlands, for reviewing the manuscript and for their valuable cooperation during this research.

The authors also extend their thanks to the Structures of Strength (SoS) platform [59] and the Centre for Unusual Collaborations (CUCo) [60] for supporting this research and the visit of the first author to Utrecht University.

Appendix A. Supplementary data

Supplementary data to this article can be found online at https://doi.org/10.1016/j.jddst.2023.104752.

References

[1] S.K. Lai, Y.Y. Wang, D. Wirtz, J. Hanes, Micro- and macrorheology of mucus, Adv. Drug Deliv. Rev. 61 (2009) 86–100, https://doi.org/10.1016/j.addr.2008.09.012.
[2] R. Bansil, B.S. Turner, Mucin structure, aggregation, physiological functions and biomedical applications, Curr. Opin. Colloid Interface Sci. 11 (2006) 164–170, https://doi.org/10.1016/j.cocis.2005.11.001.
[3] O. Lieleg, K. Ribbeck, Biological hydrogels as selective diffusion barriers, Trends Cell Biol. 21 (2011) 543–551, https://doi.org/10.1016/j.tcb.2011.06.002.
[4] T.L. Carlson, J.Y. Lock, R.L. Carrier, Engineering the mucus barrier, Annu. Rev. Biomed. Eng. 20 (2018) 197–220, https://doi.org/10.1146/annurev-bioeng-062117-121156.
[5] Z. Jia, Z. Guo, C.T. Yang, C. Prestidge, B. Thierry, "Mucus-on-Chip": a new tool to study the dynamic penetration of nanoparticulate drug carriers into mucus, Int. J. Pharm. 598 (2021), 120391, https://doi.org/10.1016/j.ijpharm.2021.120391.
[6] J.K. Sheehan, K. Oates, I. Carlstedt, Electron microscopy of cervical, gastric and bronchial mucus glycoproteins, Biochem. J. 239 (1986) 147–153, https://doi.org/10.1042/bj2390147.
[7] J.M.H. Larsson, H. Karlsson, H. Sjövall, G.C. Hansson, A complex, but uniform O-glycosylation of the human MUC2 mucin from colonic biopsies analyzed by nanoLC/MSn, Glycobiology 19 (2009) 756–766, https://doi.org/10.1093/glycob/cwp048.
[8] N. Ijssennagger, R. van der Meer, S.W.C. van Mil, Sulfide as a mucus barrier-breaker in inflammatory bowel disease? Trends Mol. Med. 22 (2016) 190–199, https://doi.org/10.1016/j.molmed.2016.01.002.
[9] R. Bansil, B.S. Turner, The biology of mucus: composition, synthesis and organization, Adv. Drug Deliv. Rev. 124 (2018) 3–15, https://doi.org/10.1016/j.addr.2017.09.023.
[10] J. Leal, H.D.C. Smyth, D. Ghosh, Physicochemical properties of mucus and their impact on transmucosal drug delivery, Int. J. Pharm. 532 (2017) 555–572, https://doi.org/10.1016/j.ijpharm.2017.09.018.
[11] R.A. Cone, Barrier properties of mucus, Adv. Drug Deliv. Rev. 61 (2009) 75–85, https://doi.org/10.1016/j.addr.2008.09.008.
[12] M.E.V. Johansson, G.C. Hansson, Immunological aspects of intestinal mucus and mucins, Nat. Rev. Immunol. 16 (2016) 639–649, https://doi.org/10.1038/nri.2016.88.
[13] C.M. Lehr, F.G.J. Poelma, H.E. Junginger, J.J. Tukker, An estimate of turnover time of intestinal mucus gel layer in the rat in situ loop, Int. J. Pharm. 70 (1991) 235–240, https://doi.org/10.1016/0378-5173(91)90287-X.
[14] C. Atuma, V. Strugala, A. Allen, L. Holm, The adherent gastrointestinal mucus gel layer: thickness and physical state in vivo, Am. J. Physiol. Gastrointest. Liver Physiol. 280 (2001) 922–929, https://doi.org/10.1152/ajpgi.2001.280.5.g922.
[15] F.J.O. Varum, E.L. McConnell, J.J.S. Sousa, F. Veiga, A.W. Basit, Mucoadhesion and the gastrointestinal tract, Crit. Rev. Ther. Drug Carrier Syst. 25 (2008) 207–258, https://doi.org/10.1615/CritRevTherDrugCarrierSyst.v25.i3.10.
[16] M.E.V. Johansson, J.K. Gustafsson, J. Holmen-Larsson, K.S. Jabbar, L. Xia, H. Xu, F. K. Ghishan, F.A. Carvalho, A.T. Gewirtz, H. Sjovall, G.C. Hansson, Bacteria penetrate the normally impenetrable inner colon mucus layer in both murine colitis models and patients with ulcerative colitis, Gut 63 (2014) 281–291, https://doi.org/10.1136/gutjnl-2012-303207.
[17] P. Paone, P.D. Cani, Mucus barrier, mucins and gut microbiota: the expected slimy partners? Gut 69 (2020) 2232–2243, https://doi.org/10.1136/gutjnl-2020-322260.
[18] L. Elberskirch, T. Knoll, A. Moosmann, N. Wilhelm, H. von Briesen, S. Wagner, A novel microfluidic mucus-chip for studying the permeation of compounds over the mucus barrier, J. Drug Deliv. Sci. Technol. 54 (2019), 101248, https://doi.org/10.1016/j.jddst.2019.101248.
[19] J.Y. Lock, T.L. Carlson, R.L. Carrier, Mucus models to evaluate the diffusion of drugs and particles, Adv. Drug Deliv. Rev. 124 (2018) 34–49, https://doi.org/10.1016/j.addr.2017.11.001.
[20] Y. Cu, W.M. Saltzman, Mathematical modeling of molecular diffusion through mucus, Adv. Drug Deliv. Rev. 61 (2009) 101–114, https://doi.org/10.1016/j.addr.2008.09.006.

[21] Y. Guo, R. Luo, Y. Wang, P. Deng, T. Song, M. Zhang, P. Wang, X. Zhang, K. Cui, T. Tao, Z. Li, W. Chen, Y. Zheng, J. Qin, SARS-CoV-2 induced intestinal responses with a biomimetic human gut-on-chip, Sci. Bull. 66 (2021) 783–793, https://doi.org/10.1016/j.scib.2020.11.015.
[22] E. Taipaleenmäki, G. Christensen, E. Brodszkij, S.A. Mouritzen, N. Gal, S. Madsen, M.S. Hedemann, T.A. Knudsen, H.M. Jensen, S.L. Christiansen, F.V. Sparsø, B. Städler, Mucopenetrating polymer – lipid hybrid nanovesicles as subunits in alginate beads as an oral formulation, J. Contr. Release 322 (2020) 470–485, https://doi.org/10.1016/j.jconrel.2020.03.047.
[23] K. Pocock, L.C. Delon, A. Khatri, C. Prestidge, R. Gibson, C. Barbe, B. Thierry, Uptake of silica particulate drug carriers in an intestine-on-a-chip: towards a better: in vitro model of nanoparticulate carrier and mucus interactions, Biomater. Sci. 7 (2019) 2410–2420, https://doi.org/10.1039/c9bm00058e.
[24] A.C. Groo, F. Lagarce, Mucus models to evaluate nanomedicines for diffusion, Drug Discov. Today 19 (2014) 1097–1108, https://doi.org/10.1016/j.drudis.2014.01.011.
[25] N. Ijssennagger, K.S. van Rooijen, S. Magnúsdóttir, J.M. Ramos Pittol, E.C. L. Willemsen, M.R. de Zoete, M.J.D. Baars, P.B. Stege, C. Colliva, R. Pellicciari, S. A. Youssef, A. de Bruin, Y. Vercoulen, F. Kuipers, S.W.C. van Mil, Ablation of liver Fxr results in an increased colonic mucus barrier in mice, JHEP Reports 3 (2021), 100344, https://doi.org/10.1016/j.jhepr.2021.100344.
[26] L. Wright, A. Wignall, S. Jõemetsa, P. Joyce, C.A. Prestidge, A membrane-free microfluidic approach to mucus permeation for efficient differentiation of mucoadhesive and mucopermeating nanoparticulate systems, Drug Deliv Transl Res (2022), https://doi.org/10.1007/s13346-022-01274-8.
[27] A. Alexiadis, K. Stamatopoulos, W. Wen, H.K. Batchelor, S. Bakalis, M. Barigou, M. J.H. Simmons, Using discrete multi-physics for detailed exploration of hydrodynamics in an in vitro colon system, Comput. Biol. Med. 81 (2017) 188–198, https://doi.org/10.1016/j.compbiomed.2017.01.003.
[28] C.A.M. Fois, T.Y.L. Le, A. Schindeler, S. Naficy, D.D. McClure, M.N. Read, P. Valtchev, A. Khademhosseini, F. Dehghani, Models of the gut for analyzing the impact of food and drugs, Adv Healthc Mater 8 (2019) 1–23, https://doi.org/10.1002/adhm.201900968.
[29] B. Jeffrey, H.S. Udaykumar, K.S. Schulze, Flow fields generated by peristaltic reflex in isolated Guinea pig ileum: impact of contraction depth and shoulders, Am. J. Physiol. Gastrointest. Liver Physiol. 285 (2003) 907–918, https://doi.org/10.1152/ajpgi.00062.2003.
[30] L. Fullard, W. Lammers, G.C. Wake, M.J. Ferrua, Propagating longitudinal contractions in the ileum of the rabbit-Efficiency of advective mixing, Food Funct. 5 (2014) 2731–2742, https://doi.org/10.1039/c4fo00487f.
[31] C.D.E. Loubens, R.G. Lentle, R.J. Love, C. Hulls, P.W.M. Janssen, Fluid mechanical consequences of pendular activity, segmentation and pyloric outflow in the proximal duodenum of the rat and the Guinea pig, J. R. Soc. Interface 10 (2013), https://doi.org/10.1098/rsif.2013.0027.
[32] Y. Wang, J.G. Brasseur, Three-dimensional mechanisms of macro-to-micro-scale transport and absorption enhancement by gut villi motions, Phys. Rev. E 95 (2017) 1–8, https://doi.org/10.1103/PhysRevE.95.062412.
[33] R.J. Love, R.G. Lentle, P. Asvarujanon, Y. Hemar, K.J. Stafford, An expanded finite element model of the intestinal mixing of digesta, Food Dig 4 (2013) 26–35, https://doi.org/10.1007/s13228-012-0017-x.
[34] A. Rygg, P.W. Longest, Absorption and clearance of pharmaceutical aerosols in the human nose: development of a CFD model, J. Aerosol Med. Pulm. Drug Deliv. 29 (2016) 416–431, https://doi.org/10.1089/JAMP.2015.1252/ASSET/IMAGES/LARGE/FIGURE12.JPEG.
[35] J. Wang, X. Shi, Molecular dynamics simulation of diffusion of nanoparticles in mucus, Acta Mech. Solida Sin. 30 (2017) 241–247, https://doi.org/10.1016/J.CAMSS.2017.03.012/METRICS.
[36] L. Kaler, K. Joyner, G.A. Duncan, Machine learning-informed predictions of nanoparticle mobility and fate in the mucus barrier, APL Bioeng 6 (2022), 26103, https://doi.org/10.1063/5.0091025/2820336.
[37] M.A. Modaresi, Numerical investigation of mucociliary clearance using power law and thixotropic mucus layers under discrete and continuous cilia motion, Biomech. Model. Mechanobiol. 22 (2023) 253–269, https://doi.org/10.1007/S10237-022-01645-7/FIGURES/20.
[38] A. Galko, S. Gsell, U. D'Ortona, L. Morin, J. Favier, Pulsated Herschel-Bulkley flows in two-dimensional channels: a model for mucus clearance devices, Phys Rev Fluids 7 (2022), https://doi.org/10.1103/PhysRevFluids.7.053301.
[39] L. Krupa, B. Bajka, R. Staroń, D. Dupont, H. Singh, K. Gutkowski, A. Macierzanka, Comparing the permeability of human and porcine small intestinal mucus for particle transport studies, Sci. Rep. (2020) 1–12, https://doi.org/10.1038/s41598-020-77129-4.
[40] Edwin N. Lightfoot, Robert Byron Bird, Warren E. Stewart, Transport Phenomena, second ed., John Wiley and Sons, New York, 2002.
[41] V. Maria, D.O. Cardoso, M. Palmira, B. Stringhetti, F. Cury, International Journal of Biological Macromolecules Mucin-polysaccharide interactions : A rheological approach to evaluate the effect of pH on the mucoadhesive properties 149 (2020) 234–245, https://doi.org/10.1016/j.ijbiomac.2020.01.235.
[42] M. Tanaka, G. Girard, R. Davis, A. Peuto, N. Bignell, Recommended table for the density of water between 0 °C and 40 °C based on recent experimental reports, Metrologia 38 (2001) 301, https://doi.org/10.1088/0026-1394/38/4/3.
[43] L. Korson, W. Drost-Hansen, F.J. Millero, L. Korson, W. Drost-Hansen, F.J. Millero, Viscosity of Water at Various Temperatures, n.d. https://pubs.acs.org/sharinguidelines.
[44] R. Syms, Rapid evaporation-driven chemical pre-concentration and separation on paper, Biomicrofluidics 11 (2017) 1–17, https://doi.org/10.1063/1.4989627.
[45] O. Lafforgue, N. Bouguerra, S. Poncet, I. Seyssiecq, J. Favier, S. Elkoun, Thermo-physical properties of synthetic mucus for the study of airway clearance, J. Biomed. Mater. Res. 105 (2017) 3025–3033, https://doi.org/10.1002/jbm.a.36161.
[46] G. Ruiz-Pulido, D.I. Medina, An overview of gastrointestinal mucus rheology under different pH conditions and introduction to pH-dependent rheological interactions with PLGA and chitosan nanoparticles, Eur. J. Pharm. Biopharm. 159 (2021) 123–136, https://doi.org/10.1016/j.ejpb.2020.12.013.
[47] R. Bansil, J.P. Celli, J.M. Hardcastle, B.S. Turner, The influence of mucus microstructure and rheology in Helicobacter pylori infection, Front. Immunol. 4 (2013) 1–12, https://doi.org/10.3389/fimmu.2013.00310.
[48] E.M. Taipaleenmäki, S.A. Mouritzen, P.S. Schattling, Y. Zhang, B. Städler, Mucopenetrating micelles with a PEG corona, Nanoscale 9 (2017) 18438–18448, https://doi.org/10.1039/c7nr06821b.
[49] P.A. Billat, E. Roger, S. Faure, F. Lagarce, Models for drug absorption from the small intestine: where are we and where are we going? Drug Discov. Today 22 (2017) 761–775, https://doi.org/10.1016/J.DRUDIS.2017.01.007.
[50] D.B. Hill, R.F. Long, W.J. Kissner, E. Atieh, I.C. Garbarine, M.R. Markovetz, N. C. Fontana, M. Christy, M. Habibpour, R. Tarran, M. Gregory Forest, R.C. Boucher, B. Button, Pathological mucus and impaired mucus clearance in cystic fibrosis patients result from increased concentration, not altered pH, Eur. Respir. J. 52 (2018), https://doi.org/10.1183/13993003.01297-2018.
[51] A.C. Groo, F. Lagarce, Mucus models to evaluate nanomedicines for diffusion, Drug Discov. Today 19 (2014) 1097–1108, https://doi.org/10.1016/j.drudis.2014.01.011.
[52] L. Liu, C. Tian, B. Dong, M. Xia, Y. Cai, R. Hu, X. Chu, Models to evaluate the barrier properties of mucus during drug diffusion, Int. J. Pharm. 599 (2021), 120415, https://doi.org/10.1016/J.IJPHARM.2021.120415.
[53] K. Schulze, Imaging and modelling of digestion in the stomach and the duodenum, Neuro Gastroenterol. Motil. 18 (2006) 172–183, https://doi.org/10.1111/J.1365-2982.2006.00759.X.
[54] C. Li, Y. Jin, Digestion of meat proteins in a human-stomach: a CFD simulation study, Innovat. Food Sci. Emerg. Technol. 83 (2023), 103252, https://doi.org/10.1016/J.IFSET.2022.103252.
[55] P. Du, N. Paskaranandavadivel, T.R. Angeli, L.K. Cheng, G. O'Grady, The Virtual Intestine: in Silico Modeling of Small Intestinal Electrophysiology and Motility and the Applications, vol. 8, Wiley Interdiscip Rev Syst Biol Med, 2016, pp. 69–85, https://doi.org/10.1002/WSBM.1324.
[56] N. Palmada, J.E. Cater, L.K. Cheng, V. Suresh, Modelling flow and mixing in the proximal small intestine, in: Proceedings of the Annual International Conference of the IEEE Engineering in Medicine and Biology Society, EMBS, 2020, pp. 2496–2499, https://doi.org/10.1109/EMBC44109.2020.9176688, 2020-July.
[57] J. Zha, S. Zou, J. Hao, X. Liu, G. Delaplace, R. Jeantet, D. Dupont, P. Wu, X. Dong Chen, J. Xiao, The role of circular folds in mixing intensification in the small intestine: a numerical study, Chem. Eng. Sci. 229 (2021), 116079, https://doi.org/10.1016/J.CES.2020.116079.
[58] C. Li, J. Xiao, X.D. Chen, Y. Jin, Mixing and emptying of gastric contents in human-stomach: a numerical study, J. Biomech. 118 (2021), 110293, https://doi.org/10.1016/J.JBIOMECH.2021.110293.
[59] (n.d. SoS. http://structuresofstrength.com/. (Accessed 2 May 2023).
[60] (n.d. Cuco. https://www.unusualcollaborations.com/. (Accessed 2 May 2023).